



HAL
open science

Impact of the clusterization on the solubility of oxygen and vacancy concentration in nickel: A multi-scale approach

Damien Connétable, Matthieu David, Aurélien Prillieux, David J. Young,
Daniel Monceau

► To cite this version:

Damien Connétable, Matthieu David, Aurélien Prillieux, David J. Young, Daniel Monceau. Impact of the clusterization on the solubility of oxygen and vacancy concentration in nickel: A multi-scale approach. *Journal of Alloys and Compounds*, 2017, 708, pp.1063-1072. 10.1016/j.jallcom.2017.03.018 . hal-01579504

HAL Id: hal-01579504

<https://hal.science/hal-01579504>

Submitted on 31 Aug 2017

HAL is a multi-disciplinary open access archive for the deposit and dissemination of scientific research documents, whether they are published or not. The documents may come from teaching and research institutions in France or abroad, or from public or private research centers.

L'archive ouverte pluridisciplinaire **HAL**, est destinée au dépôt et à la diffusion de documents scientifiques de niveau recherche, publiés ou non, émanant des établissements d'enseignement et de recherche français ou étrangers, des laboratoires publics ou privés.



Open Archive TOULOUSE Archive Ouverte (OATAO)

OATAO is an open access repository that collects the work of Toulouse researchers and makes it freely available over the web where possible.

This is an author-deposited version published in : <http://oatao.univ-toulouse.fr/>
Eprints ID : 18117

To link to this article : DOI: 10.1016/j.jallcom.2017.03.018
URL : <http://dx.doi.org/10.1016/j.jallcom.2017.03.018>

| |
|--|
| <p>To cite this version : Connétable, Damien and David, Matthieu and Prillieux, Aurélien and Young, David J. and Monceau, Daniel <i>Impact of the clusterization on the solubility of oxygen and vacancy concentration in nickel: A multi-scale approach.</i> (2017) Journal of Alloys and Compounds, vol. 708. pp. 1063-1072. ISSN 0925-8388</p> |
|--|

Any correspondence concerning this service should be sent to the repository administrator: staff-oatao@listes-diff.inp-toulouse.fr

Impact of the clusterization on the solubility of oxygen and vacancy concentration in nickel: A multi-scale approach

Damien Connétable ^{a,*}, Matthieu David ^a, Aurélien Prillieux ^{a,b}, David Young ^b, Daniel Monceau ^a

^a CIRIMAT UMR 5085, CNRS-INP-UPS, ENSIACET 4, allée Émile Monso, BP 44362, F-31030, Toulouse Cedex 4, France

^b School of Materials Science and Engineering, The University of New South Wales, Sydney, NSW, 2052, Australia

A B S T R A C T

Combining thermodynamic concepts with first-principles calculations, we study the solubility of oxygen atoms (O) in nickel. In our approach, we include the possible formation of oxygen clusters (O_n) and vacancies-oxygens clusters (VO_n and V_2O_n). We show that the vacancy-oxygens interactions are strong (approximately 1 eV) and would induce a large concentration of clusters in fcc-Ni. The use of a thermodynamic model, within a grand canonical approach, allows calculation of the vacancy concentration, including these VO_n clusters, as a function of O concentration, for different temperatures. We find that at low temperatures (below 600 K), a small content of oxygen (in appm) strongly modifies the vacancy concentration, increasing the total vacancy concentration in the metal by many orders of magnitude more than the thermal vacancy concentration. The vacancy concentration is thus directly controlled by the oxygen content in the metal. At high temperatures, the effect is reduced, becoming negligible near the melting point. These results show the strong impact of interstitial atoms on the vacancy concentration. The influence of the vacancy formation energy is also discussed.

Keywords:

DFT
Thermodynamic model
Nickel
Oxygen
Clusters

1. Introduction

Predicting the concentration and the diffusion mechanisms of interstitial elements, like C, O, H, or point defects are major problems in solid state physics. Due to thermodynamical problems (time of equilibration in particular), their concentrations have usually been measured only at high temperatures. The concentration, $C[X]$, is then interpolated by Arrhenius or Sieverts' laws at high temperatures. One then extrapolates values at low T from parameters evaluated at high temperature. Nonetheless, recent studies on the effects of temperature and interactions between defects and interstitial atoms point to the need to modify the use of simple mechanisms (only free atoms). For example, as illustrated in recent work on hydrogen in nickel [1–4], the hydrogen interactions with vacancies modifies the vacancy concentration as well as their diffusion. Recently equivalent work on oxygen, carbon and nitrogen in iron [5,6] has shown the same trend.

For H atoms, the mechanism, described by Fukai [7], is

characterized by a super-abundant vacancies concentration (labeled SAVs): under high pressures of hydrogen and at high temperatures, the vacancy concentration is significantly increased. The use of simulations based on the density functional theory (DFT) have allowed an understanding of the atomic processes. First-principles studies have thus confirmed that, in many metals, vacancies can trap high H content (see work on Fe [8–10], Al [11,12], Mg [12], Ti [13] or Ni [1,4]): from 6 to 10 atoms according to the crystallographic structure and the metal. This strong binding and multiple occupancy of hydrogen can enhance the formation energy of the defects. However, DFT simulations alone are not able to predict the global concentration and fraction of defects according to the temperature and the chemical potential (grand canonical approach) in a metal. The use of thermodynamic concepts [2,6,10] allows solution of this difficulty. Thus, it has been seen that a large segregation of H atoms in the vacancies increases significantly the concentration of vacancies, especially at low and intermediate temperatures (below 600 K). It has also been shown that in nickel, hydrogen-vacancy interactions enhance the diffusion mechanisms of solutes or self-interstitial atoms at low temperatures [3].

In the case of oxygen in nickel, this mechanism has not been studied. Nonetheless, as we will see, an equivalent SAVs

* Corresponding author.

E-mail address: damien.connetable@ensiacet.fr (D. Connétable).

mechanism should appear too. From a technological point of view, in the lifetime prediction of structures, oxide layer growth modelling involves incorporating the oxygen concentration and diffusivity during oxidation processes. It is thus crucial to predict the quantity of O atoms and vacancy concentration in the metal, to know where they are located and in which form.

Furthermore, from an experimental point of view, there is still a debate concerning the oxygen solubility in nickel. Two sets of data are often opposed in the literature, with different apparent results: those of Park et al. [14] and the results of Seybolt [15] and Alcock [16] measurements. More recently, Jullian et al. [17] proposed a new set of data and a new interpretation of the experimental measurements. Without discussing details at this point, an additional aim is to compare our work with theirs.

From a theoretical point of view, solubility energy of oxygen referred in the literature (see references given in Ref. [18]) do not fit well with experimental measurements, a direct comparison between experimental and theoretical energies is difficult. Experimentally, different aspects should be taken into account in the measurement of oxygen concentration in the metal: is the metal directly in equilibrium with the oxidising gas (for low oxygen chemical potentials)? Is oxygen in the metal in equilibrium with the gas or the oxide? According to the temperature and the O₂ pressure in the gas, summarised in the Ellingham diagrams, the oxygen concentration is thus controlled by the solubility energy of the O atoms in the metal, but also the possible clusterization. Moreover, when an oxide is formed on the surface of the metal, the oxygen chemical potential in the metal is controlled by the equilibrium with the oxide. The limit of solubility is thus controlled differently if the oxide is present or not. It is thus important to analyse concentrations according to the chemical potential of oxygen. The purpose of this work is to understand how oxygen-vacancy interactions could alter the vacancy concentration and the total oxygen concentration in nickel, and more generally to provide an understanding of the elementary mechanisms.

We identify multiple aims of this study: (i) evaluate effects of the formation of different type of clusters (O_n, VO_n and V₂O_n) on the vacancy concentration, (ii) predict the vacancy concentration according to the oxygen concentration or its chemical potential and (iii) finally, obtain under which form we can found the O atoms in the metal. To achieve this goal, we used DFT energies in a thermodynamic model, taking into account reduced configurations. Of course, all these points are important for O diffusion in the metal, for stress corrosion cracking understanding and internal oxidation kinetics.

The manuscript is organised as following: we first present computational details, we then discuss insertion of O atoms in the bulk, before presenting results of the interactions of one vacancy and one oxygen. We conclude the DFT part with the results on multi-segregation of O atoms to a vacancy. Then, the effect of oxygen potential on the clusters' concentration and finally the oxygen concentration parametrization are discussed within the thermodynamic model.

2. Computational details

2.1. First-principles approach

The present calculations were performed based on the density functional theory (DFT) using VASP (Vienna *ab initio* simulation package [19]). The generalised gradient approximations (PBE [20]) for the exchange and correlation functionals were used. Projector augmented wave (PAW) pseudo-potentials [21] were used to describe Ni and O atoms. The magnetic moments taken into account in all calculations are necessary to avoid errors, as nickel is

ferromagnetic. Large super-cells (3 × 3 × 3, i.e., 108 Ni atoms) were used to compute converged energies and reduce image interactions. The inter-atomic forces and the stress were relaxed. We ensured that atomic forces are always smaller than 0.02 eV/Å on the O and Ni atoms. The plane-wave cut-off energy was set to 600 eV, and 6 × 6 × 6 Monkhorst-Pack mesh grids [22] were used to sample the Brillouin zone. These criteria are necessary to reach accurate values in the case of the insertion of the O atoms and produced segregation energies converged to within 5 meV. The vibrations of atoms were evaluated by diagonalizing the dynamical matrix corresponding to the only degrees of freedom of oxygen (nickel atoms were kept frozen and only O frequencies were computed). They were computed on 3 × 3 × 3 supercells, using a finite displacements approach, where the relative displacements are fixed equal to 0.01.

Pseudo-potentials were tested and validated for the reference states, fcc-Ni and O₂. For nickel, we obtained a cohesive energy equal to −4.88 eV/atom (for an experimental value equal to −4.44 eV/atom [23]), a lattice parameter (a₀) equal to 3.52 Å (3.52 Å [23]), and a magnetic moment equal to 0.62 μ_B (0.61, experimentally). For O₂, the dissociation energy is found to be equal to −3.41 eV/atom (−2.60 eV/atom [23]) and the diatomic distance to 1.23 Å (1.21 Å [24]). This discrepancy could induce mistakes in the segregation energies calculated in the following. Atomic vibrations in O₂ (1597 cm^{−1}), computed using a frozen mode approximation taking a relative displacement equal to 0.01, are in excellent agreement with experimental data (1580 cm^{−1} [24]).

2.2. Thermodynamic model

To take into account the interactions of the O atoms with defects (vacancy) in a statistical approach, we employed a multi-scale approach using DFT energies. In our approach, we considered that point defects (vacancy, O atoms, clusters...) are in equilibrium thermodynamically, related to their formation energies. The formation energy of the defect (D) is thus defined as:

$$H_f[D] = \mathcal{E}[D] - \mu[\text{Ni}] \cdot \delta n_{\text{Ni}} - \frac{1}{2} \mu[\text{O}_2] \cdot \delta n_{\text{O}} \quad (1)$$

where $\mathcal{E}[D] = E_o[D] - E_o[\text{bulk}]$ is the grand canonical energy of the defect (free atoms, vacancy and clusters). The total energy of the system with the point defect ($E_o[D]$) and the perfect system ($E_o[\text{bulk}]$) are the DFT values. $\mu[X]$ corresponds to the chemical potential of the specie X (nickel and oxygen), and δn_X is the difference of composition in X element between a system with and without point defect. For a system, which contains one vacancy and m O atoms, we have δn_{Ni} and δn_{O} are equal to -1 and $+m$, respectively.

In a grand canonical potential approximation, at the thermodynamical equilibrium, we obtained different sets of equations for clusters and interstitials sites. Here, we only considered low concentrations ($C \ll 1$), the model is also equivalent to a LTE (Low

Table 1

Formation energies (H_f , in eV/atom) and frequencies (in meV and cm^{−1}) of the O atoms. In addition, experimental and theoretical values extracted to the literature.

| Site | H_f | charge | ω | |
|--------------|--|--------|----------|------------------|
| | eV/atom | e | meV | cm ^{−1} |
| octahedral | 0.46 ^a /0.31 ^b /−0.22 ^c | +0.8 | 51 | 418 |
| tetrahedral | 0.63 ^a /0.47 ^b /0.13 ^c | +0.8 | 68 | 549 |
| substitution | +1.46 ^a /1.10 ^c | +0.9 | unstable | |

^a PBE functional, VASP present work.

^b PW91 functional, VASP [18].

^c LDA-PZ81 functional, VASP [26], corrected by the DFT formation energy of O₂.

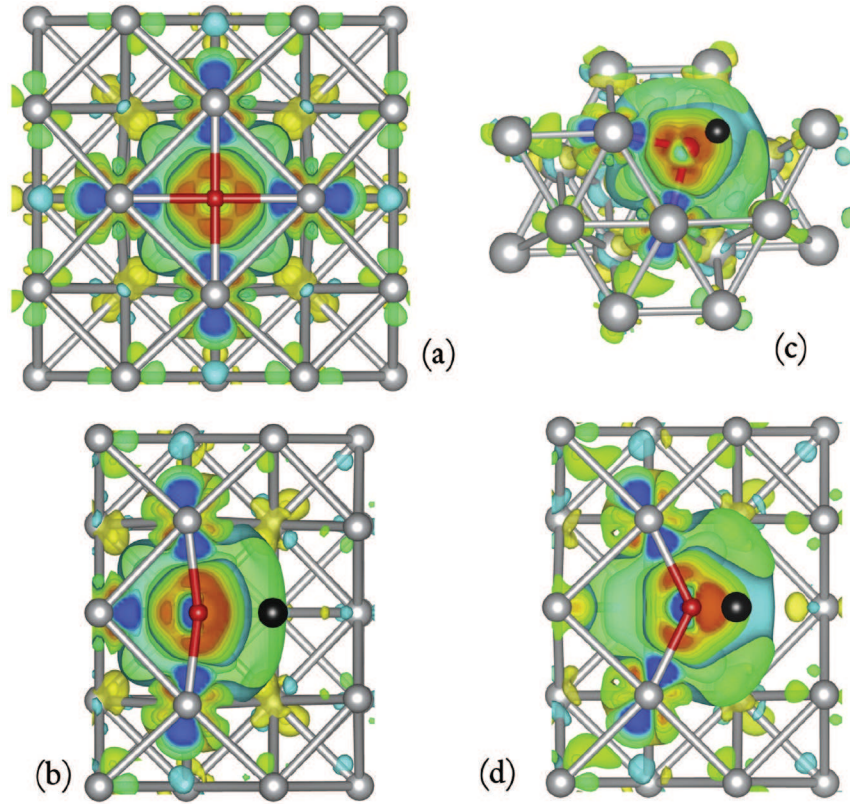


Fig. 1. Charge density difference when an O atom is in the octahedral position (a), in VO₁ (b), VT₁ (c) and VO_v (d) configurations. The scale goes from blue (negative) to red (positive); red spheres indicate atom positions. The black ball represents the position of the vacancy. (For interpretation of the references to colour in this figure legend, the reader is referred to the web version of this article.)

temperature expansion) approach as used in previous works [6]. For each type of cluster Y (O _{n} , VO _{n} and V₂O _{n}) the concentration ($C_j[Y]$) of the configuration j is given by:

$$C_j[Y] \approx \mathcal{S}_j[Y] \exp\left(-\frac{H_f^j[Y]}{kT}\right) \quad (2)$$

where $\mathcal{S}_j[Y]$ represents the number of equivalent configurations of the Y cluster of type j . To a first-order approximation, $C_j[Y]$ is proportional to the number of ways to form the cluster (\mathcal{S}_j^Y).

The total concentration of monovacancies ($C_{tot}[V]$), divacancies ($C_{tot}[V_2]$) and oxygen concentration ($C_{tot}[O]$) are thus expressed by:

$$\begin{cases} C_{tot}[V] = \sum_{n,j} C_j[V_1 X_n] \\ C_{tot}[V_2] = \sum_{n,j} C_j[V_2 X_n] \\ C_{tot}[O] = \sum_{n,m,j} n C_j[V_m X_n] \end{cases} \quad (3)$$

The equations are thus controlled by the temperature (T) and the chemical potential of O ($\mu[O]$), or the total oxygen concentration ($C_{tot}[O]$) in the metal.

2.3. Preliminary results

We first studied the solubility of O atoms in Ni. Formation

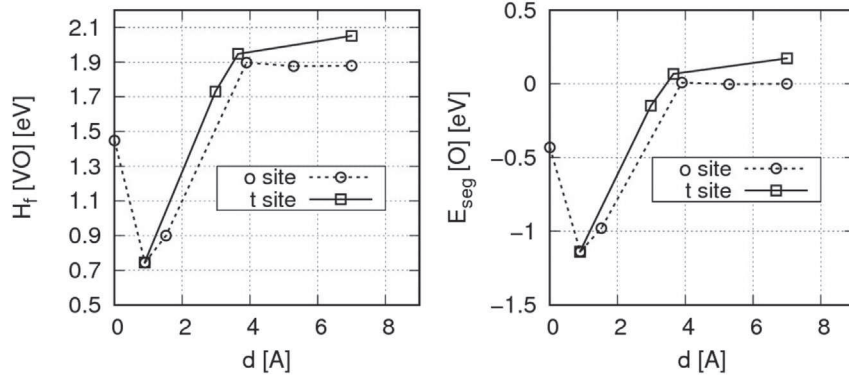


Fig. 2. Schematic evolution of the formation ($H_f[VO]$, left) and segregation ($E_{seg}[O]$, right) energies of the O-vacancy interactions.

Table 2

Formation and segregation energies (H_f and E_{seg} respectively, measured in eV/atom), frequencies (ω , in meV) of the O atoms around the vacancy (V). In addition, we give the zero-point energy (ZPE, measured in meV), the vibrational formation energy (F_{vib} , in meV) and the Bader's charge on O atoms.

| | d_{OV} | H_f | E_{seg} | ω | ZPE | F_{vib} | e |
|---------|----------|-------|-----------|----------|-----|-----------|------|
| s | 0.00 | 1.427 | -0.431 | unstable | — | — | +0.9 |
| t_1 | 0.89 | 0.745 | -1.138 | 37/37/39 | 56 | +11 | +0.9 |
| o_v | 0.90 | 0.745 | -1.138 | 28/32/32 | 45 | 0 | +1.0 |
| o_1 | 1.52 | 0.900 | -0.980 | 16/56/56 | 64 | +19 | +1.0 |
| t_2 | 2.98 | 1.730 | -0.150 | 48/53/54 | 78 | +33 | — |
| t_3 | 3.65 | 1.947 | 0.067 | — | — | — | — |
| o_2 | 3.90 | 1.897 | 0.008 | 45/51/54 | 75 | +30 | — |
| o_3 | 5.28 | 1.876 | -0.004 | — | — | — | — |
| o'_3 | 5.28 | 1.888 | 0.009 | — | — | — | — |
| $o+V_1$ | ∞ | 1.879 | 0 | 51/51/51 | 77 | +32 | +0.8 |
| $t+V_1$ | ∞ | 2.051 | 0.172 | 68/68/68 | 102 | +57 | +0.8 |
| V_1 | — | 1.427 | — | — | — | — | — |

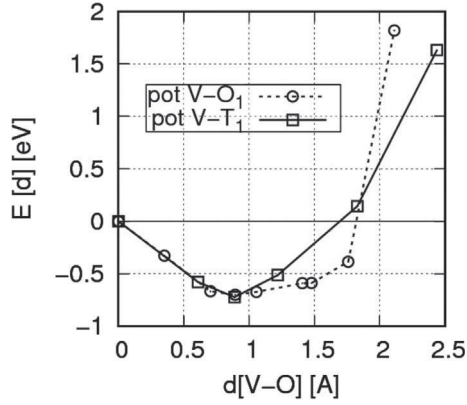


Fig. 3. Schematic energy landscapes in the vacancy: dependence of the energy ($E[d]$) on the distance vacancy-oxygen (d , in Å). The origin (in energy) is the substituted position: along the vacancy- t_1 direction ($V-t_1$), and the vacancy- o_1 - o_v direction ($V-o_1$). Energies were calculated fixing oxygen atoms in different positions, without relaxation.

energies (H_f^0 , where “0” means computed using the O_2 energy, i.e. $\mu[O] = \mu^0[O] = E_o[O_2]/2$) of the tetrahedral, octahedral and substituted (s) sites are listed in Table 1. The charge transfer (using Bader's analysis [25]) and the oxygen vibrations in nickel are also given.

The most stable configuration is the octahedral site with a solubility energy equal to 0.46 eV. The t site is only 0.17 eV higher in

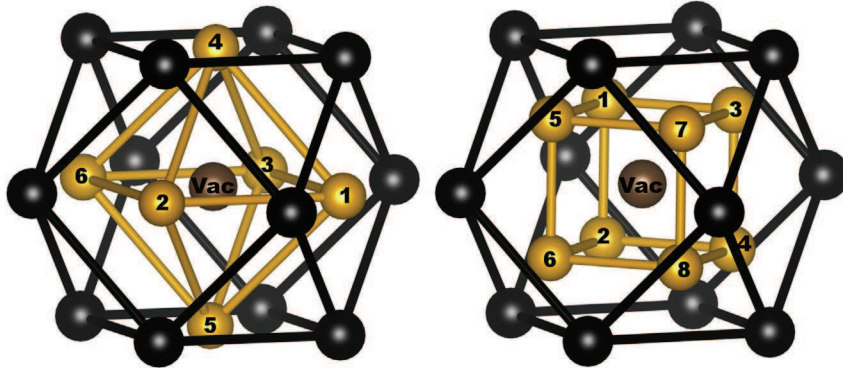


Fig. 4. Schematic of the different positions of O atoms in tetrahedral (right) and octahedral (left) positions inside the vacancy: O atoms are depicted in yellow, Ni in black and the vacancy in brown. (For interpretation of the references to colour in this figure legend, the reader is referred to the web version of this article.)

energy than the o site. The substituted site is significantly higher in energy (≈ 1 eV) than interstitial sites. This result is in satisfactory agreement with earlier calculations, computed with different functionals, i.e., GGA-PW91 [18] or LDA-PZ81 [26]. The LDA values are slightly different from the one found using GGA functionals. We must note that, although the LDA functional provides ostensibly accurate values of vacancy formation energies at 0 K, it is well established that the LDA is unsuitable to describe accurately the properties of metals. Recently, Glensk et al. [27] have proposed an explanation for the disagreement between experimental and theoretical formation energies. They showed that, in Al and Cu, the vacancy formation energy (E_f^{1v}) varies with temperature: a low temperature correctly calculated by DFT but difficult to measure and a high temperature (in agreement with the experimental result) value.

No direct comparison of the theoretical solubility energies with experimental data is possible at this stage. In the literature, different sets of experimental results can be found for measurements done at high temperature (from 800 to 1400 °C). In the first set of data, the oxygen concentration, reported by Seybolt [15] and Alcock [16], increases when the temperature decreases. The second one was more recently reported by Park et al. [14], and is considered by the community to be more accurate than the first.

From early high temperature measurements, oxygen concentration follows Sieverts' law [28]:

$$C[O] = \exp\left(-\frac{\Delta S_s^0}{R}\right) \sqrt{\frac{p_{O_2}}{p_o}} \exp\left(-\frac{\Delta H_s^0}{RT}\right). \quad (4)$$

Standard enthalpies (ΔH_s^0) and entropies (ΔS_s^0) of solution of oxygen gas in fcc-Ni are reported in the experimental literature: -182 kJ/mol (-1.89 eV) and -70 J/mol.K, respectively for Park et al. and -244 kJ/mol (-2.53 eV) and -117 J/mol.K, respectively for Seybolt and Alcock. Clearly, our calculated values are far removed from the measured ones. At this stage, our model based on oxygen only inside the interstitial sites seems to be unsuitable to describe the physics. In the theoretical literature, we can find some suggested explanation, comparing insertion energy (with atomic oxygen as reference state) to try to understand the disagreement. The main uncertainty is the value of the reference state (O_2), where the DFT is wrong.

We also evaluated the zero-point-energy (ZPE) corrections for oxygen inside the bulk, using the following expression: $\sum_i \hbar\omega_i/2$ (at 0 K). We obtained one frequency for O atoms, with a degeneracy of three, equal to 418 and 549 cm^{-1} (i.e., ≈ 51 and 68 meV) for the *octa* and *tetra* sites, respectively. From these frequencies, we calculated the ZPE using following expression:

Table 3

Formation (H_f^0) and segregation (E_{seg}^{seg}) energies (in units of eV) of the V_1O_m clusters. For the segregation energy, the number of the O atom removed is given in brackets. In the case of multi-segregation in t_1 and o_v sites, O atoms moved through o_1 sites, we then do not compute the segregation energy, the number of equivalent configurations $\mathcal{S}_i[VO_m]$ are also listed.

| m | sites | \mathcal{S}_i | config. | H_f | E_{seg} |
|-----|-------|-----------------|---------|--------|------------------------|
| — | o | 4 | | 0.455 | 0 |
| — | t | 8 | | 0.628 | +0.172 |
| 0 | — | — | | 1.427 | — |
| 1 | o_1 | 6 | 1 | 0.908 | -0.980 (1) |
| | o_v | 6 | 1 | 0.745 | -1.138 (1) |
| | t_1 | 8 | 1 | 0.743 | -1.140 (1) |
| 2 | o_1 | 3 | 1,6 | 0.190 | -1.174 (2) |
| | | 12 | 1,2 | 0.458 | -0.906(6) |
| | o_v | 3 | 1,6 | 0.128 | -1.072(2) |
| | | 12 | 1,2 | 0.457 | -0.906(6) ^a |
| | t_1 | 12 | 1,2 | 0.346 | -0.852(2) |
| | | 12 | 1,7 | 0.767 | -0.431(7) |
| | | 4 | 1,8 | 0.129 | — |
| 3 | o_1 | 12 | 1-3 | -0.194 | -0.839(1)/-1.107(3) |
| | | 8 | 1,2,4 | -0.052 | -0.697(4) |
| | t_1 | 24 | 1-3 | 0.963 | — |
| | | 24 | 1,2,8 | -0.056 | — |
| | | 8 | 1,4,6 | -0.047 | — |
| 4 | o_1 | 3 | 1-3,6 | -0.691 | -0.952(6) |
| | | 12 | 1-4 | -0.653 | -0.915(4)/-1.057(3) |
| | t_1 | 2 | 1,4,6,7 | 3.302 | — |
| | | 6 | 1-4 | 0.712 | — |
| | | 24 | 1,2,3,8 | 0.664 | — |
| | | 24 | 1,2,4,8 | 1.584 | — |
| | | 8 | 1,2,3,5 | 0.089 | — |
| | | 6 | 1,2,7,8 | 0.638 | — |
| 5 | o_1 | 6 | 1-5 | -1.157 | -0.922(1)/-0.960(5) |
| | t_1 | 24 | 1-5 | 0.198 | — |
| | | 24 | 1,3-6 | 2.077 | — |
| | | 8 | 1-3,5,8 | 0.152 | — |
| 6 | o_1 | 1 | 1-6 | -1.654 | -0.952(6) |
| | t_1 | 12 | 1-6 | 0.200 | — |
| | | 12 | 1-5,8 | 1.526 | — |
| | | 4 | 1,3-6,8 | 2.294 | — |
| 7 | t_1 | 8 | 1-7 | 0.226 | — |
| 8 | t_1 | 1 | 1-8 | 4.231 | — |

^a The O atoms move through the o_1 configurations.

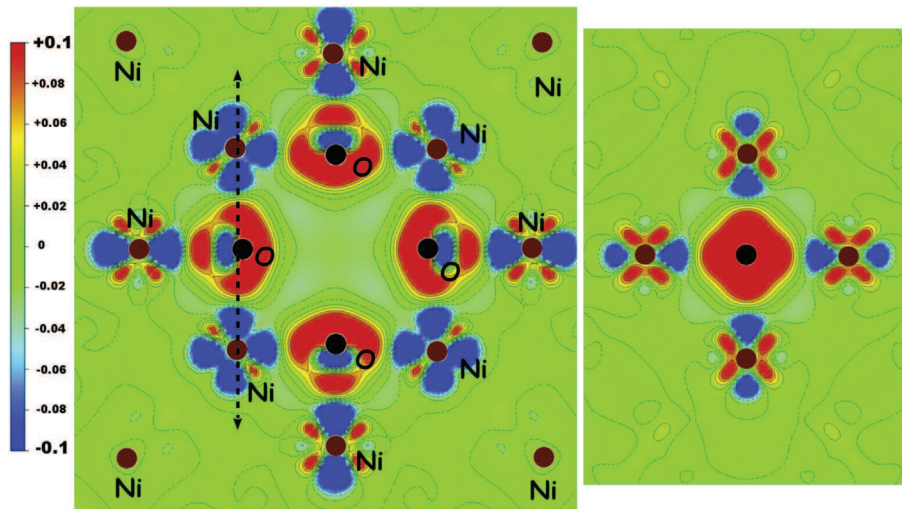


Fig. 5. Contour maps of the $\Delta\rho$ electron density distribution for VO_6 . In black is depicted O atoms and in brown Ni atoms: in red (blue) are depicted the positive (negative) contribution. Right figure represents the plot in the plane defined by the arrow in the left figure. (For interpretation of the references to colour in this figure legend, the reader is referred to the web version of this article.)

Table 4

Formation (H_f) and segregation (E_{seg}) energies (in units of eV) of the V_1O_m according to the number of O atoms ($m \leq 8$) in the cluster on o_2 sites. The number of equivalent configurations ($\mathcal{S}_i[VO_m]$) are also reported.

| m | $\mathcal{S}_i[VO_m]$ | H_f | E_{seg} |
|-----|-----------------------|--------|-----------|
| 7 | 8 | -1.647 | -0.448 |
| 8 | 28 | -1.768 | -0.577 |
| 9 | 56 | -1.957 | -0.644 |
| 10 | 70 | -2.144 | -0.642 |
| 11 | 56 | -2.395 | -0.706 |
| 12 | 28 | -2.676 | -0.737 |
| 13 | 8 | -3.003 | -0.783 |
| 14 | 1 | -3.372 | -0.824 |

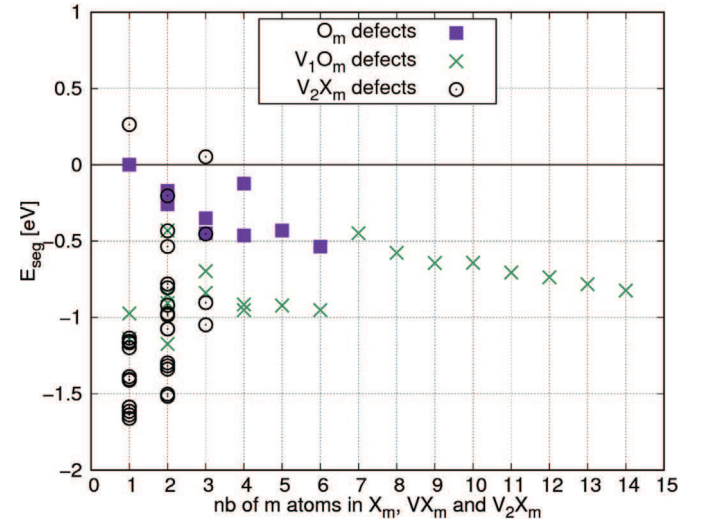


Fig. 6. Segregation energies of V_pX_m clusters, according to the number of O atoms in the clusters.

Table 5

Formation (H_f) and segregation (E_{seg}) energies (in units of eV) of the O_m clusters according to the number of oxygens in the defect, O atoms are in octahedral sites. The number of equivalent configurations ($\mathcal{N}[O_n]$) are also reported. The configuration † corresponds to the first-nearest-neighbouring position (1nn), and ‡ the 2nn. We also report an additional clusters (labelled "compact"), where all O atoms are in 1nn configurations without a Ni atom inside the pyramid formed by oxygens.

| m | | $\mathcal{N}[O_n]$ | H_f | E_{seg} |
|-----|---------|--------------------|-------|-----------|
| 1 | 1 | 6 | 0.455 | — |
| 2 | 1, 6† | 3 | 0.741 | -0.170 |
| | 1, 2‡ | 12 | 0.653 | -0.258 |
| 3 | 1-3 | 12 | 0.757 | -0.351 |
| | 1, 2, 4 | 8 | 0.660 | -0.448 |
| 4 | 1-3, 6 | 3 | 0.992 | -0.124 |
| | 1-4 | 12 | 0.653 | -0.463 |
| | Compact | 6 | 0.685 | -0.431 |
| 5 | 1-5 | 6 | 0.573 | -0.536 |
| 6 | 1-6 | 1 | 1.060 | 0.032 |

$$ZPE = F_{vib}[Ni + O] - F_{vib}[Ni] - \frac{1}{2}F_{vib}[O_2] \quad (5)$$

where F_{vib} are the vibrational contribution of the enthalpy energy. In a first-order approximation, we neglect the influence of oxygen on nickel vibrations, and the ZPE can be reduced to:

$$ZPE \approx \hbar\omega[O \text{ in Ni}]/2 - \frac{1}{2}\hbar\omega[O_2]/2 \quad (6)$$

where $\omega[O \text{ in Ni}]$ is the sum of O frequencies in the metal, and $\omega[O_2]$ is the O_2 vibration. The ZPE for the *octa* and *tetra* sites are therefore low ≈ 77 and 102 meV, respectively. When we take into account the ZPE of the O_2 molecule (equal to 45 meV) the correction at 0 K of the formation energy is *in fine* low: 32 and 57 meV. In comparison, in the case of the H atom [1], the ZPE represents 30% of the total enthalpy energy.

For the substitutional site, the analysis of frequencies shows that it is an unstable configuration (there are three imaginary frequencies). These facts are in contradiction with the results of Garuchet [29]: when a O atom is put in a substitutional position, the vacancy is partially restored to form a vacancy-oxygen pair, by a displacement of the O atom from the substituted site to another (see above).

To enlarge our DFT results, we also considered the dumbbell configuration (with one O and one Ni atom) as suggested by Garuchet [29]. We found, that, after minimisation of forces, both atoms regained their stable positions, i.e., the octahedral configuration and the nickel site. We found that the dumbbell is not a stable defect in nickel.

To conclude, we analyse the charges around atoms using Bader's criteria [25]. In the metal, the charge transfer is in favour of the O atoms, which become partially charged ($+0.9$ e). This result is illustrated by the differential charge density distributions, $\Delta\rho = \rho(Ni + O) - \rho(Ni) - \rho(O)$, plotted in Fig. 1(a). Only first nearest neighbouring nickel atoms transfer a part of their charges on the O atom, which should weaken their bonds. We clearly see a charge

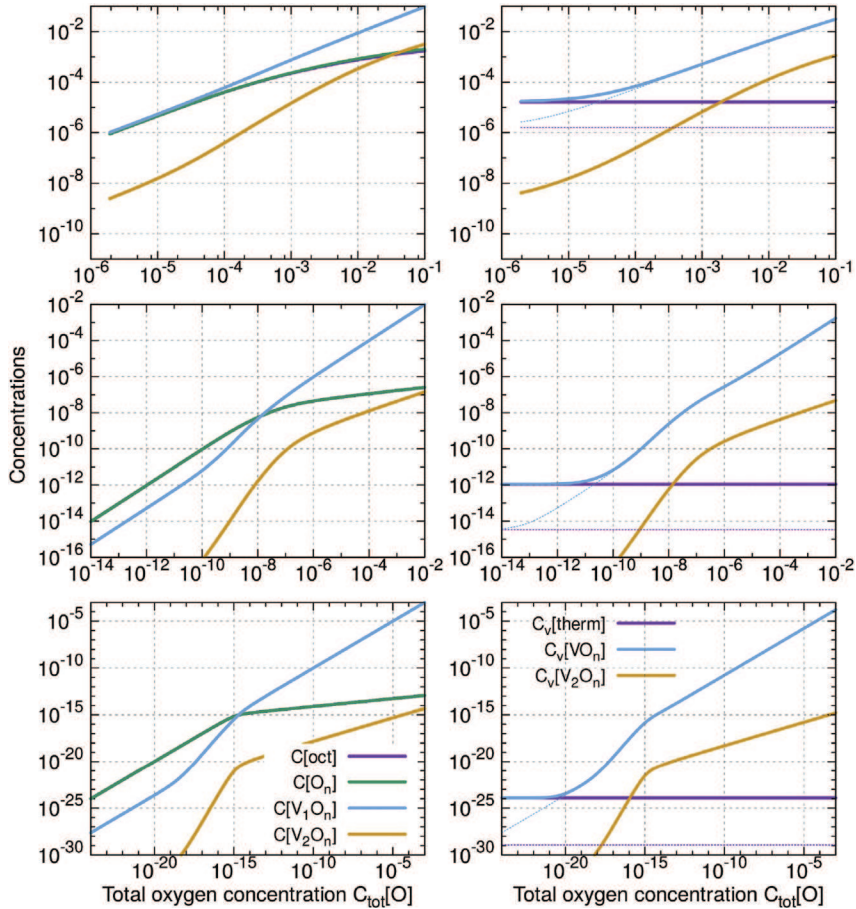


Fig. 7. Variation of the oxygen (left) and clusters (right) concentration as a function of the total oxygen concentration $C_{tot}[O]$ at 300, 600 and 1500 K in each type of clusters O_m , VO_m and V_2O_m . Dot dashed lines represent the results calculated with the experimental value (1.73 eV) of the vacancy formation energy instead the DFT value (1.43 eV).

transfer from both the surrounded nickel and the O atoms to the space between them, which proves a covalent nature of chemical bonding.

3. Analysis of oxygen-vacancy interactions

To analyse the vacancy-oxygen interactions, we first consider the formation and segregation energies according to the O-vacancy distance (d_{OV}). Fig. 2 show the change in these energies with d_{OV} . In Table 2, we list the formation energies (H_f) and the segregation energies (E_{seg}) and the O frequencies. The segregation energy given by the equilibrium:



is expressed by:

$$E_{seg}[VO_n] = E_o[(m-1)Ni + O_n] + E_o[mNi] - E_o[(m-1)Ni + O_{n-1}] - E_o[mNi + O_{octa}] \quad (8)$$

where $E_o[pNi + X]$ is the DFT value of the super-cell containing p Ni atoms and a cluster/atom X . E_{seg} corresponds to the energy gained/lost when an O atom is trapped by an existing VO_{n-1} cluster from an octahedral position. Within the PBE functional, the formation energy of the vacancy is equal to 1.43 eV, in agreement with the literature, a value slightly higher than the one obtained using the PW91 functional (1.40 eV, see Refs. [1,18]), but which should better match the low temperature value of the formation energy, as suggested by results of Glensk et al. [27]. As explained above, at high temperatures, we will consider in the following the experimental value (1.7 eV).

When an O atom is located inside the monovacancy, its energy decreases significantly. Its segregation energy is thus large, approximately -1.1 eV, and the vacancy is partially restored: the O atoms move from the nickel site through an intermediate position, neither tetrahedral, nor octahedral. The ZPE in these cases (see Table 2) is always low and is, in the following, neglected. We find that the stable configuration for one oxygen in a vacancy is twice: the ‘‘tetrahedral’’ site (see Fig. 4) and a site located (labeled o_v) between the vacancy and the ‘‘true’’ octahedral site (labeled o_1). The octahedral position (o_1) corresponds to a local minimum, as already observed by Fang et al. [26]. To illustrate in detail this result, the energy landscapes were plotted in Fig. 3 between the t_1 (o_1) site and the substitution site. The t_1 and o_v configurations are stable. From results presented in Fig. 2, we also note that, in the vicinity of the vacancy, the energy converges quickly with that of bulk behavior. Beyond the third-nearest position, O atoms and vacancies interact only slightly.

The charge transfer is always in favor of the O atom: the O atoms are slightly charged ($\approx +1e^-$) in the vacancy, as illustrated on the contour maps plotted in Fig. 1 b, c and d. This suggests a strong interaction between the ‘‘surface’’ of the vacancy and O atom.

4. Formation of VO_m clusters

4.1. Inside the vacancy

We have shown in the previous section that the segregation of one O atom in the vacancy is strong, up to -1 eV. We now investigate multi-oxygen segregation in the vacancy. Non-equivalent configurations of VO_n were studied in detail (restricting in first neighbour shell of the vacancy), including o_v , t_1 and o_1 sites, see Fig. 4. The formation energies and corresponding segregation energies were all computed. These formation energies are then used next in the thermodynamical

formalism to compute VO_m concentrations. The energy values are summarised in Table 3.

The most striking result is the favourable energetics of trapping multiple O atoms in a vacancy, as already observed in the case of other interstitials elements in metals (Ni, Fe, Pd, W, Al ...) [1,4,6,30–33]. DFT results show that up to six O atoms can segregate inside a vacancy. In these configurations, only octahedral o_1 sites are occupied. The segregation energy thus is nearly constant, approximately -0.95 eV, independently of the number of O atoms in the sites. These configurations are all stable (no imaginary frequencies). We also found that the o_v sites should be filled only for small O contents. Beyond three oxygens in a vacancy, O atoms move to the o_1 sites, which can be explained by the O-O repulsion. In the case of the tetrahedral configurations, apart the VO_8 cluster which has a large formation energy, most of O atoms in t_1 move to the o_1 sites. These configurations are thus unstable, even in the case of VO_2 . Indeed, when two O atoms are too close (as in multi- t_1 configurations), it is not possible to form O-O bonds inside one vacancy, atoms are always repelled, due to the charge around oxygen. The mean O-O distance is then significantly larger than in the O_2 molecules.

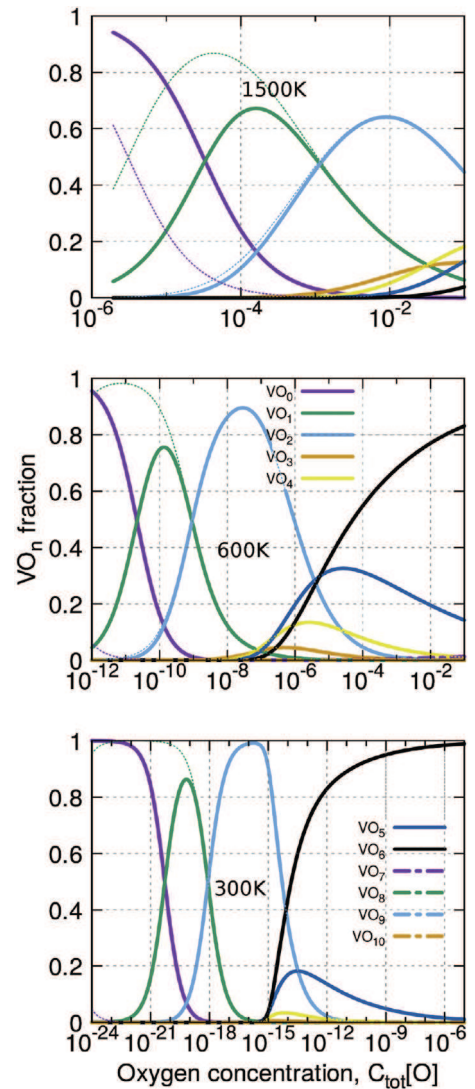


Fig. 8. Distribution of VO_n clusters at 300, 600 and 1500 K (bottom to top). Dot dashed lines are the results calculated with the experimental value of the vacancy formation energy.

Finally, the nature of the chemical bond in VO_6 was examined by plotting the electron density distribution maps (see Fig. 5). We note a charge transfer from the p states of the first-nearest neighbouring Ni atoms to the p and d states of O and Ni atoms, respectively (confirmed by the electronic density of states, not shown here). One part of the charge density is in direction of the vacancy, as already observed in Fig. 1. The VO_6 defect is stable, all O atoms interacting with their nearest Ni atoms to form bonds.

4.2. Segregation around the vacancy

Here all o_1 sites in first-nearest neighbour shell of the vacancy are already filled and second nearest neighbour segregation around the vacancy was then studied. O atoms were then progressively added to o_2 sites. To simplify, we only considered one configuration for each m , where m is greater than seven (only octahedral sites were considered). Interactions between the O atoms in o_2 sites where ignored as the distance between these positions are large enough. The energies of VO_m are given in Table 4.

In the preliminary section, we showed that the o_2 sites have a higher energy than the o_1 site ($\Delta \approx 1$ eV). We now find that when all o_1 sites are already fully filled, o_2 sites became energetically favoured. The segregation energy is nearly constant, $\approx -0.6 / -0.8$ eV, but significantly smaller than the segregation in first-nearest position in the vacancy. These results suggest that vacancies could be considered as an ideal place for the nucleation of oxides when O concentrations is high, and that clusters of large sizes ($n > 6$) should be not necessarily thermodynamic favoured in comparison with small.

5. Formation of V_2O_m clusters

We then considered some clusters composed with two vacancies V_2O_m , where O atoms are only placed in octahedral sites. We limited our study to the case where m is smaller than 3. Since 2NN divacancy ($H_f = 2.93$ eV) is less stable than 1NN ($H_f = 2.80$ eV), only segregation inside 1NN divacancies is presented, even if some tests were conducted in the case of 2NN for information. These results on empty divacancies are in agreement with previous works, see Ref. [18] and cited references. All configurations for $m = 1$ and 2 were considered in the first-neighbouring of the divacancy. Results are depicted in Fig. 6.

The segregation energy of O atoms in 1NN is high: it is in the range of $[-1.6; -1.1]$ eV in V_2 and $[-1.5; -0.5]$ eV in V_2O . In comparison with the value obtained in the case of mono-vacancy, the gain is greater. This will increase significantly the number of divacancies in the metal.

6. Formation of O_m clusters

The last type of clusters considered are the O_m . We restrict to the cases where O atoms are only located in the octahedral sites. We considered the same configurations as for VO_m clusters, without the vacancy. DFT energies are given in Table 5 and included in Fig. 6.

We show that O atoms could also form O_m clusters. The first-nearest neighbours interaction (configuration labelled \dagger in Table 5) is attractive (-0.26 eV) but significantly smaller than when there is a vacancy (-1.1 eV). We also note that, up to 5 atoms, the segregation energies become negative, but not with 6 O atoms, the

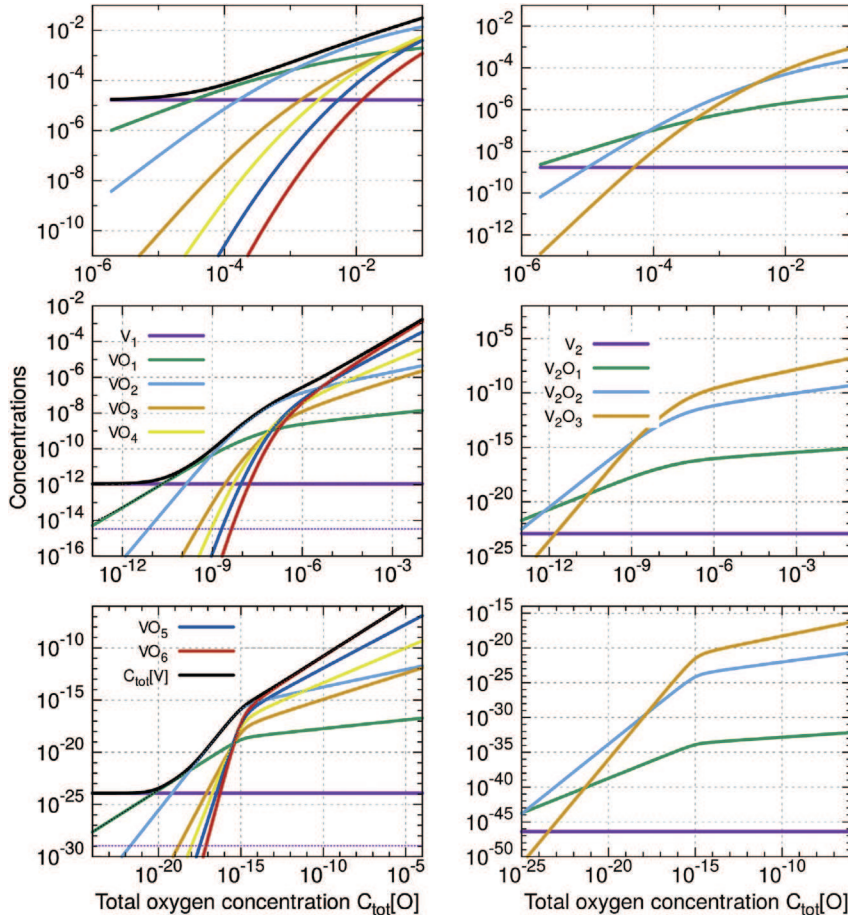


Fig. 9. Concentration of VO_m and V_2O_m clusters and for each m value as a function of T , where O atoms are in the vacancy.

cluster remains less stable. An energetic model, based on lower clusters, can not explain this result. From a statistical point of view, we will see that large O_m clusters, do not exist in the metal, others non compact clusters can thus be neglected.

7. Stability of defect content

We now used all these DFT energies in the statistical equations to compute the concentration of each type of defect according to the temperature. For a given oxygen chemical potential ($\mu[O]$) there is only one value of $C_{tot}[O]$, results are also presented as a function of the O concentration ($C_{tot}[O]$) in the metal. The effect of the vacancy formation energy is investigated.

Fig. 7 shows the numerical results, for three temperatures (300, 600 and 1500 K), of the oxygen concentration in the each type of clusters and the concentration of clusters. We identify two ranges of results according to T: at low temperatures, a small content of oxygen would strongly modify the cluster concentrations, and at high temperatures, the effect is reduced.

We can use experimental data for oxygen concentration. Above 1100 K, the oxygen concentration is between 200 and 500 apm of O atoms (see Ref. [17]). Our results predict first the total vacancy concentration $C_{tot}[V]$ is approximately 1–2 times larger than without oxygen, see thermal equilibrium concentration of vacancy, $C_v[therm]$ in Fig. 7. In these temperatures and oxygen concentrations ranges oxygens are mainly located in clusters VO_m , which are composed with only one and two oxygens, see Fig. 8 on top. The changing of the value of the vacancy formation energy only

qualitatively modifies our result (one order of magnitude). Larger clusters (VO_m , $n > 3$) are filled at only very high O content (beyond 10^{-2}). One find that O_m clusters have significant lower concentrations than other clusters, see Fig. 10, except the free O atom, O_1 . Finally, the concentration in divacancies are also increased, but their concentrations retains lower than VO_m clusters (Fig. 9).

At lower temperature, experimental data are missing: the equilibrium state is difficult to attain, and measured concentrations are low (\leq ppm). If we apply Sieverts' law (using for instance the Park-Altstetter parameters), one should have $2 \cdot 10^{-11}$ and 10^{-6} O concentrations (in the limit of solubility) in the metal at 300 and 600 K, respectively. We see that, even for these low values, the impact on vacancy concentration is huge (see Fig. 7), and the total vacancy concentration ($C_{tot}[V]$) is controlled by the cluster concentrations. At ambient temperatures, as the majority of O atoms should be located inside clusters, (the main defect is VO_6 , see Fig. 8) one should have quantitatively the same order of magnitude of clusters and oxygen. $C_{tot}[V]$ is also much larger than that of oxygen-free thermal vacancies: the total vacancy concentration is seen to be 12 orders of magnitude larger than expected (10^{-25} at 300 K). The vacancy concentration is then six times lower than oxygen concentration. O_m , V_2O_m and VO_l (where l greater than 7) clusters do not change the results (see Figs. 9 and 10). Large mono vacancies are not promoted due to their lower segregation energies. Concerning the divacancies with oxygen, they always have strong concentrations in comparison to the empty ones, which have too low concentrations, whatever the temperature. At high temperature (beyond 1200 K) in the range of experimental oxygen

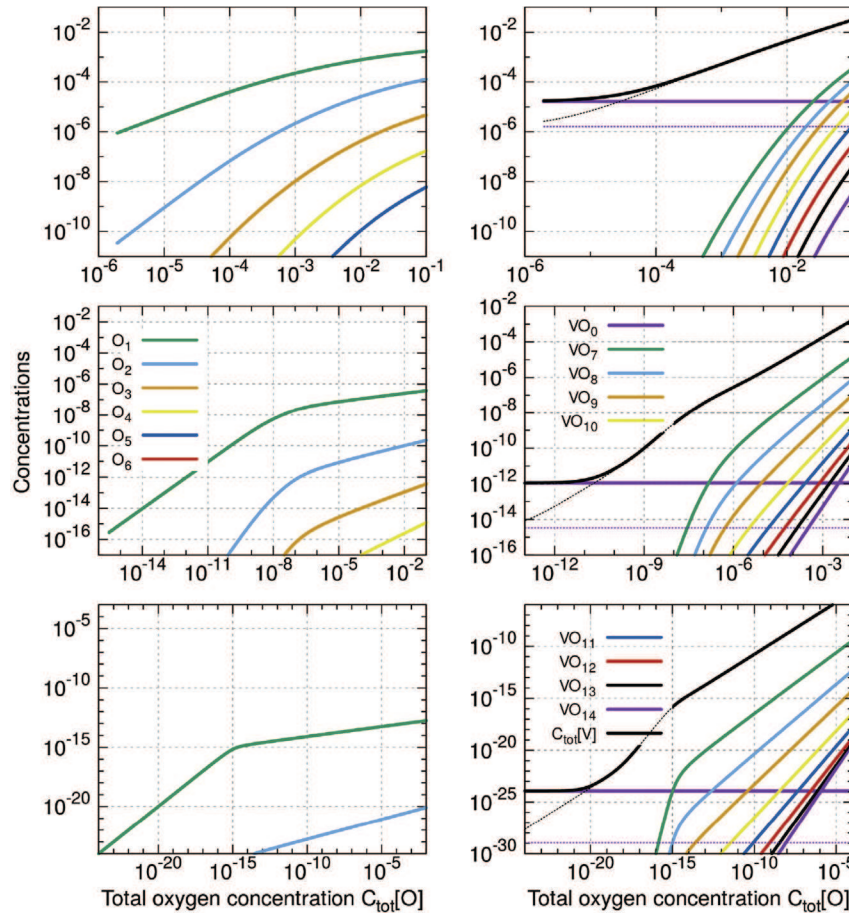


Fig. 10. Concentration of O_m and VO_m ($m \leq 8$) clusters and for each m value as a function of T.

concentrations, V_2O and V_2O_2 have non negligible concentrations in comparison to VO_m . We can expect that they play a role in the diffusion mechanisms of oxygen.

8. Conclusion

We presented a multi-scale modelling of oxygen solubility in nickel, including vacancy-oxygens clusters. DFT configurations and energies of clusters (O_m , V_m and V_2O_m) are then used in a statistical model to compute the cluster concentrations. We show that from an energetic point of view, O atoms interact strongly with the mono-vacancies, with a segregation energy equal to approximately 1 eV. The cluster is composed of a vacancy that can be filled up to a total of six oxygens in the octahedral positions. Without vacancy, the compact O_m clusters are also stable but with a segregation energy smaller than for clusters with vacancies. Clusters composed of divacancies have also large segregation energies.

Using a statistical approach, we computed the oxygen and vacancy concentrations taking into account the clusters' formation. We show that the clusterization effects are relevant at low temperature (up to 600 K): the strong oxygen-vacancy interactions induce the formation of large numbers of clusters, and therefore, a large content of vacancies. For oxygen concentrations in the range of ppm at., the vacancy concentration is huge with respect to the temperature. Most of the O atoms form clusters and the total amount of clusters is of the same order of magnitude as the O concentration. At high temperatures (above 1200 K), the effect becomes negligible. The nature of the type of defects where the oxygen is found in the metal changes according to the oxygen concentration and the temperature. One can thus expect that the entropy of solubility can be modified according to the experimental conditions.

Acknowledgments

This work was performed using HPC resources from CALMIP (Grant 2014-, 2015- and 2016-p0912).

References

- [1] D. Connétable, Y. Wang, D. Tanguy, Segregation of hydrogen to defects in nickel using first-principle calculations: the case of self-interstitials and vacancies, *J. Alloys Compd.* 614 (2014) 211–220.
- [2] D. Tanguy, Y. Wang, D. Connétable, Stability of vacancy-hydrogen clusters in nickel from first principles calculations, *Acta Mater.* 78 (2014) 135–143.
- [3] Y. Wang, D. Connétable, D. Tanguy, Hydrogen influence on diffusion in nickel from first-principles calculations, *Phys. Rev. B* 91 (2015) 094106.
- [4] R. Nazarov, T. Hickel, J. Neugebauer, *Ab initio* study of h-vacancy interactions in fcc metals: implications for the formation of superabundant vacancies, *Phys. Rev. B* 89 (2014) 144108, <http://dx.doi.org/10.1103/PhysRevB.89.144108>.
- [5] C. Barouh, T. Schuler, C.-C. Fu, M. Nastar, Interaction between vacancies and interstitial solutes (c, n, and o) in α -fe: from electronic structure to thermodynamics, *Phys. Rev. B* 90 (2014) 054112.
- [6] T. Schuler, C. Barouh, M. Nastar, C.-C. Fu, Equilibrium vacancy concentration driven by undetectable impurities, *Phys. Rev. Lett.* 115 (2015) 015501, <http://dx.doi.org/10.1103/PhysRevLett.115.015501>.
- [7] Y. Fukai, *The Metal-hydrogen System: Basic Bulk Properties*, second ed., Springer-Verlag Berlin and Heidelberg GmbH & Co. K, 2003.
- [8] Y. Tateyama, T. Ohno, Stability and clusterization of hydrogen-vacancy complexes in α -fe: an *ab initio* study, *Phys. Rev. B* 67 (2003) 174105.
- [9] W. Counts, C. Wolverton, R. Gibala, First principles energetics of hydrogen traps in α fe: points defects, *Acta Mater.* 58 (2010) 4730.
- [10] R. Nazarov, T. Hickel, J. Neugebauer, First principles study of the thermodynamics of hydrogen vacancy interaction in fcc iron, *Phys. Rev. B* 82 (2010) 224104.
- [11] C. Wolverton, V. Ozolins, M. Asta, Hydrogen in aluminum: first-principles calculations of structure and thermodynamics, *Phys. Rev. B* 69 (2004) 144109.
- [12] L. Ismer, M.S. Park, A. Janotti, C. VandeWalle, Interactions between hydrogen impurities and vacancies in mg and al: a comparative analysis based on dft, *Phys. Rev. B* 80 (2009) 184110.
- [13] D. Connétable, J. Huez, E. Andrieu, C. Mijoule, First-principles study of the migration process of hydrogen and vacancy in titanium, *J. Phys. Condens. Matter* 23 (2011) 405401, <http://dx.doi.org/10.1088/0953-8984/23/40/405401>.
- [14] J.-W. Park, C. Altstetter, The diffusion and solubility of oxygen in solid nickel, *Metall. Trans. A* 18A (1987) 43.
- [15] A. Seybolt, dissertation, Yale university, New Haven, CT, 1936.
- [16] C.B. Alcock, P.B. Brown, Physicochemical factors in the dissolution of thorium in solid nickel, *Metall. Sci. J.* 3 (1969) 116.
- [17] D. Jullian, A. Prillieux, J. Zhang, D. Hibbert, D. Young, Oxygen solubility in Fe-Ni alloys at high temperature in Rhines packs and in gas mixtures, in: *Corrosion and Prevention 2015*, Australasian Corrosion Association, Adelaide, 2015.
- [18] D. Connétable, E. Andrieu, D. Monceau, First-principles nickel database: energetics of impurities and defects, *Comput. Mater. Sci.* 101 (2015) 77–87.
- [19] G. Kresse, J. Hafner, *Ab initio* molecular dynamics for liquid metals, *Phys. Rev. B* 47 (1993) 558R.
- [20] J. Perdew, K. Burke, M. Ernzerhof, Generalized gradient approximation made simple, *Phys. Rev. Lett.* 78 (1997) 1396.
- [21] G. Kresse, D. Joubert, From ultrasoft pseudopotentials to the projector augmented-wave method, *Phys. Rev. B* 59 (1999) 1758.
- [22] H. Monkhorst, J. Pack, Special points for the brilluoin zone integrations, *Phys. Rev. B* 13 (1976) 5188.
- [23] C. Kittel, *Introduction to Solid State Physics*, Wiley, New York, 1996.
- [24] K.P. Huber, G. Herzberg, *Molecular Spectra and Molecular Structure. IV. Constants of Diatomic Molecules*, Van Nostrand Reinhold, New York, 1979.
- [25] G. Henkelman, A. Arnaldsson, H. Jónsson, A fast and robust algorithm for bader decomposition of charge density, *Comput. Mater. Sci.* 36 (2006) 354.
- [26] H. Fang, S. Shang, Y. Wang, Z. Liu, D. Alfonso, D. Alman, Y. Shin, C. Zou, A. van Duin, Y. Lei, G. Wang, First-principles studies on vacancy-modified interstitial diffusion mechanism of oxygen in nickel, associated with large-scale atomic simulation techniques, *J. Appl. Phys.* 115 (2014) 043501.
- [27] A. Glensk, B. Grabowski, T. Hickel, J. Neugebauer, Breakdown of the arrhenius law in describing vacancy formation energies: the importance of local anharmonicity revealed by *Ab initio* thermodynamics, *Phys. Rev. X* 4 (2014) 011018, <http://dx.doi.org/10.1103/PhysRevX.4.011018>.
- [28] A. Sieverts, The absorption of gases by metals, *Z. für Met.* 21 (1929) 37–46.
- [29] S. Garruchet, O. Politano, P. Arnoux, V. Vignal, Diffusion of oxygen in nickel: a variable charge molecular dynamics study, *Solid State Commun.* 150 (9–10) (2010) 439–442, <http://dx.doi.org/10.1016/j.ssc.2009.12.012>.
- [30] M. Ji, C.-z. Wang, K.-m. Ho, S. Adhikari, K.R. Hebert, Statistical model of defects in al-h system, *Phys. Rev. B* 81 (2010) 024105, <http://dx.doi.org/10.1103/PhysRevB.81.024105>.
- [31] A.-Y. Gao, Y.-L. Liu, Z.-H. Dai, C. Duan, Elucidating hydrogen assisting vacancy formation in metals: Mo and nb as examples, *Eur. Phys. J. B* 86 (8) (2013), <http://dx.doi.org/10.1140/epjb/e2013-40552-x>.
- [32] N. Fernandez, Y. Ferro, D. Kato, Hydrogen diffusion and vacancies formation in tungsten: density functional theory calculations and statistical models, *Acta Mater.* 94 (2015) 307–318, <http://dx.doi.org/10.1016/j.actamat.2015.04.052>. URL, <http://www.sciencedirect.com/science/article/pii/S1359645415003043>.
- [33] C.-C. Fu, F. Willaime, *Ab initio* study of helium in α -Fe: dissolution, migration, and clustering with vacancies, *Phys. Rev. B* 72 (2005) 064117, <http://dx.doi.org/10.1103/PhysRevB.72.064117>.